View metadata, citation and similar papers at core.ac.uk

brought to you by CORE

provided by University of Regensburg Publication Server

ZAAC
Zeitschrift für anorganische und allgemeine Chemie

DOI: 10.1002/zaac.201800142

ARTICLE

Synthesis and Characterization of Ag_2MnSnS_4, a New Diamond-like Semiconductor

Daniel Friedrich,[a] Sebastian Greil,[a] Theresa Block,[b] Lukas Heletta,[b] Rainer Pöttgen,[b] and Arno Pfitzner*[a]

Dedicated to Prof. Wolfgang Bensch on the Occasion of his 65th Birthday

Abstract. Phase pure Ag_2MnSnS_4 was synthesized from the elements using standard high-temperature solid-state methods. Its crystal structure was solved from single-crystal X-ray diffraction data collected from a pseudo-merohedrally twinned crystal as well as by Rietveld refinement of X-ray powder diffraction data. Ag_2MnSnS_4 crystallizes in the monoclinic space group *Pc* (no. 7) with the unit cell parameters a = 6.651(1), b = 6.943(1), c = 10.536(2) Å, β = 129.15(1)°, V = 337.3(1) Å^3, and Z = 2. The tetrahedraly compound crystallizes in a superstructure of the wurtzite type and the tetrahedra volumes are in good agreement with the model for diamond-related compounds derived from the wurtzite structure type. The red semiconductor Ag_2MnSnS_4 has an optical bandgap of E_g = 2.0 eV and is stable up to its peritectic decomposition temperature of approximately 700 °C. Ag_2MnSnS_4 is a Curie–Weiss paramagnet with an experimental magnetic moment of μ_{exp} = 5.4(1) μ_B per manganese atom. Antiferromagnetic ordering is detected at a Néel temperature of T_N = 8.8(1) K. ^{119}Sn Mößbauer spectra at 78 K underline the single tetrahedrally coordinated Sn^{IV} site (δ = 1.34(1) mm·s^{-1}). The 6 K spectrum (magnetically ordered state) reveals a small transferred magnetic hyperfine field of 1.02(1) T.

Introduction

The first tetrahedral compound in literature is stannite (Cu_2FeSnS_4),[1] whose name also describes a structure-type of quaternary tetrahedral compounds that are derived from sphalerite. Starting in 1970 several more of these quaternary compounds were synthesized. Their structures were either related to the sphalerite structure-type or could be derived from the wurtzite structure-type.[2–4] The latter materials are consequently called wurtz-stannite type compounds. Usually, these compounds exhibit semiconducting properties and may be used as diamond-like semiconductors (DLS).[5–6] In recent years, this class of compounds received a lot of attention as these materials exhibit a broad range of interesting physicochemical properties depending on the chemical composition of the solids. Their optical and electrical properties make them very promising photovoltaic materials. Especially $Cu(In,Ga)(S,Se)_2$ is in the focus of photovoltaics due to its high efficiency.[7–8] The quaternary compound Cu_2ZnSnS_4[9] is also investigated as photovoltaic material. *Steinhagen* suggested nanocrystals of Cu_2ZnSnS_4 to use them as a cheaper route to photovoltaics,[10] and *Scragg* found that the bandgap (1.49 eV) of Cu_2ZnSnS_4 is quite close to the optimum for the usage in solar cells.[11] Non-centrosymmetric, diamond-like semiconductors are also very interesting materials in the field of non-linear optics.[12,13] Interesting examples in this field are for example GaAs, GaP, $AgGaQ_2$ (Q = S, Se),[13,14] and quaternary compounds like $Li_2MnSnSe_4$[15] or Li_2CdGeS_4.[16]

Recently, tetrahedral networks deviating from this diamond-like topology ($LiGaGe_2Se_6$, $Li_2In_2MQ_6$ with M = Si, Ge, Q = S, Se) were also reported to have interesting non-linear optical properties.[17,18] Furthermore, materials containing Mn^{2+}, Fe^{2+} or Co^{2+} are of special interest due to their magnetic properties.[19–22] *Nénert* discussed the potential of $Cu_2M^{II}M^{IV}S_4$ as multiferroics,[22] as such materials show coupling of both their magnetic and their electronic properties. The authors found that several of these compounds are possible multiferroics with high polarization due to their symmetry and structural considerations. In detail Cu_2MnGeS_4 and Cu_2MnSnS_4 were investigated and both compounds show a linear magnetoelectric effect.[6] The same arguments should hold true for Ag_2MnSnS_4, since its crystal structure is quite similar to that of Cu_2MnGeS_4. The crystal structures of such diamond-like tetrahedral compounds can usually be derived from the two different polymorphs of zinc sulfide. Normal-valent tetrahedral compounds are also called adamantane compounds.[20] Deviations of an average of four valence electrons per atom will cause structural distortions as for example shown for Cu_3TeS_3Cl. This compound has an excess of two valence electrons, which are located in a lone electron pair at the Te^{4+} cation.[23] Possible combinations of elements for such adamantane compounds can be derived via cross-substitution as shown by *Parthé*.[24]

It has been shown that a superstructure related either to the wurtzite-type or to the sphalerite-type results in ternary and

* Prof. Dr. Arno Pfitzner
Fax: +49 941 943 4551
E-Mail: arno.pfitzner@chemie.uni-regensburg.de
[a] Institut für Anorganische Chemie
Universität Regensburg
Universitätsstraße 31
93040 Regensburg, Germany
[b] Institut für Anorganische und Analytische Chemie
Westfälische Wilhelms-Universität Münster
Corrensstraße 30
48149 Münster, Germany

Supporting information for this article is available on the WWW under **http://dx.doi.org/10.1002/zaac.201800142** or from the author.

 © 0000 WILEY-VCH Verlag GmbH & Co. KGaA, Weinheim

multinary materials of this class depending on the volume differences of the constituting tetrahedra $[MQ_4]$.[25,26] According to this model the volume differences of the tetrahedra $[MQ_4]$ have a strong impact on the structure type. For small volume differences a sphalerite-type related structure will occur, and wurtzite-type related structures are preferred in case of differences greater than a critical value. A different model suggests wurtzite-type related superstructures for silver compounds and sphalerite-type related superstructures for copper compounds, thus referring to the smaller ionic radius of copper.[27] It also suggests that the wurtzite structure-type should be preferred at higher temperatures. This trend describes some compounds quite well, though it is not as quantitative as the model presented above.[27] A third model[28] refers to the *c*/*a*-ratio of tetrahedral compounds. At room temperature there is an ideal ratio of 1.633 for wurtzite-type structures. Those compounds having a smaller ratio prefer a wurtzite-type structure, while those having a larger ratio will consequently prefer the sphalerite-type structure. This ratio decreases at higher temperatures and therefore describes why wurtzite-type modifications tend to be more stable at higher temperatures. Further articles have been published which discuss the volumes of tetrahedral compounds and their influence on the structure type.[25–32]

Herein, we present the synthesis and crystal structure determination of the adamantane compound Ag_2MnSnS_4, which has been investigated earlier.[21,54] However, only its antiferromagnetic properties and an erroneous orthorhombic metric were reported at that time. It has recently been mentioned also by *Lekse*, but no reasonable structure model is known to date.[33] Very recently a structure determination was reported assuming orthorhombic symmetry and neglecting the monoclinic symmetry of the title compound thus leading to quite significantly enlarged *R*-values.[34]

Results and Discussion

Crystal Structure Determination of Ag_2MnSnS_4

The crystal structure of Ag_2MnSnS_4 was solved from single-crystal X-ray diffraction data collected at 20 °C. Ag_2MnSnS_4 crystallizes in the monoclinic space group *Pc* (no. 7) with a = 6.651(1), b = 6.943(1), c = 10.536(2) Å, β = 129.15(1)°, V = 337.3(1) Å^3, and Z = 2. An initial structure solution in the orthorhombic space group $Pmn2_1$ resulted in unusually high *R* values (see also reference[34]). Therefore, a symmetry reduction was considered, i.e., monoclinic symmetry with pseudo-merohedral twinning similar to Li_2ZnSnS_4.[35] This symmetry reduction leads to the monoclinic space group *Pn* (no. 7), a non-standard setting of *Pc*. The resulting R_1 value dropped significantly from R_{ortho} = 0.0490 to R_{mono} = 0.0348. An additional twofold-axis was introduced to take the pseudo-symmetry into account. The corresponding twin law (in *Pn*), 1 0 0, 0 –1 0, 0 0 –1, dropped the final *R* values to R_1(all data) = 0.0283 and wR_2(all data) = 0.0518. The non-standard setting *Pn*, however, was only used to emphasize the symmetry relations to the orthorhombic supergroup $Pmn2_1$. For the following discussions, the structure of Ag_2MnSnS_4 is presented in the standard setting *Pc*. The final crystallographic data and experimental details of the data collection are listed in Table 1. The atomic coordinates, equivalent displacement parameters, and anisotropic displacement parameters are listed in Table 2 and Table 3. Table 4 shows selected bond lengths and angles.

Table 1. Crystallographic data for Ag_2MnSnS_4.

	Ag_2MnSnS_4	
Formula weight M /g·mol^{-1}	517.61	
Color	black	
Crystal system	monoclinic	
Space group	*Pc* (no. 7)	*Pn* (no. 7)
Lattice constants from single crystal		
a /Å	6.651(1)	6.651(1)
b /Å	6.943(1)	6.943(1)
c /Å	10.536(2)	8.171(2)
β /°	129.15(1)	90.00(3)
Unit cell volume V /Å^3	377.3(1)	
Number of formula units Z	2	
Calculated density ρ /g·cm^{-3}	4.56	
Diffractometer	STOE IPDS I	
Temperature T /°C	20(1)	
Wavelength λ /Å	0.71073	
Absorption coeff. μ(Mo-K_α) / mm^{-1}	11.0	
θ range /°	2.93–25.18	
Index range	$-7 \le h \le 7$ $-8 \le k \le 8$ $-12 \le l \le 12$	
No. of reflections collected	3366	
Independent reflections	1356	
R_{int}, R_σ	0.0250, 0.0248	
Completeness to θ = 25°	99.9 %	
Absorption correction	Numerical, XRED [36], X-SHAPE [37]	
Structure solution	Charge flipping, ShelXT [38]	
Structure refinement	Full-matrix least-squares on F^2, ShelXL-2018 [39]	
Twin law	1 0 –2, 0 –1 0, 0 0 –1	1 0 0, 0 –1 0, 0 0 –1
Twin fraction	22.8 %	
Data / restraints / parameters	1356, 2, 75	
Flack parameter	–0.01(2)	
GooF, F(000)	0.974, 466	
R_1, wR_2 [$I > 2\sigma(I)$]	0.0243, 0.0283	
R_1, wR_2 [all data]	0.0506, 0.0518	
Extinction coefficient G_{iso}	0.0041(4)	
Largest diff. peak and hole / e·Å^{-3}	0.76, –0.71	

The competition between the space groups $Pmn2_1$ and *Pn* has already been described by *Parthé* in 1969.[2] The authors mentioned that for Cu_2CdGeS_4, also an adamantane compound, it is difficult to determine the right space group. Furthermore, they already pointed out that the diffraction patterns are identical for both space groups. This also holds true for Ag_2MnSnS_4. The X-ray powder diffraction patterns for the orthorhombic and for the monoclinic structure models therefore cannot be distinguished. The symmetry relations between $Pmn2_1$ and *Pn*, as well as the relations to the wurtzite structure type are shown in a *Bärnighausen*-tree (see Figure 1).[40]

Consequently, the *R* values for the pattern fit of the Rietveld refinement of Ag_2MnSnS_4 were practically identical for the space groups $Pmn2_1$ and *Pc*. However, similar to the single-

 © 0000 WILEY-VCH Verlag GmbH & Co. KGaA, Weinheim

Table 2. Atomic coordinates and isotropic displacement parameters U_{eq} [a)] /Å^2 for Ag_2MnSnS_4 (20 °C) in the space group *Pc*.

Atom	Wyckoff site	s.o.f.	x	y	z	U_{eq}
Ag1	2*a*	1	0.2532(7)	0.6679(3)	0.2505(4)	0.0457(6)
Ag2	2*a*	1	0.0000(7)	0.1565(2)	0.0002(4)	0.0455(4)
Mn	2*a*	1	0.7428(2)	0.3250(4)	0.2469(7)	0.0244(6)
Sn	2*a*	1	0.4982(5)	0.1741(1)	0.5002(3)	0.0194(2)
S1	2*a*	1	0.8501(7)	0.1856(5)	0.4918(5)	0.0263(7)
S2	2*a*	1	0.3870(7)	0.1528(4)	0.0062(5)	0.0251(7)
S3	2*a*	1	0.6267(7)	0.6581(6)	0.2410(5)	0.0245(7)
S4	2*a*	1	0.1226(7)	0.3220(6)	0.2581(5)	0.0265(8)

a) U_{eq} is defined as one third of the trace of the orthogonalized U_{ij} tensor.

Table 3. Anisotropic displacement parameters U_{ij} /Å^2 for Ag_2MnSnS_4 (20 °C) in the space group *Pc*.

Atom	U_{11}	U_{22}	U_{33}	U_{23}	U_{13}	U_{12}
Ag1	0.042(1)	0.047(1)	0.046(1)	0.008(1)	0.027(1)	0.009(1)
Ag2	0.045(1)	0.047(1)	0.047(1)	–0.002(1)	0.030(1)	0.000(1)
Mn	0.025(1)	0.024(1)	0.024(1)	–0.007(2)	0.016(1)	–0.007(2)
Sn	0.018(1)	0.020(1)	0.020(1)	0.000(1)	0.012(1)	0.001(1)
S1	0.023(1)	0.032(1)	0.027(2)	0.003(2)	0.017(1)	0.004(2)
S2	0.025(2)	0.021(1)	0.026(2)	0.002(2)	0.015(1)	–0.001(2)
S3	0.029(2)	0.022(1)	0.025(2)	0.004(2)	0.018(1)	0.005(2)
S4	0.023(2)	0.029(2)	0.027(2)	0.001(2)	0.016(1)	0.002(2)

Table 4. Selected interatomic distances /Å and angles /° for Ag_2MnSnS_4 (20 °C).

Distance /Å		Angle /°	
Ag1–S1^{i}	2.534(6)	S1^{i}–Ag1–S3	111.3(2)
Ag1–S3	2.550(5)	S1^{i}–Ag1–S2^{ii}	111.4(2)
Ag1–S2^{ii}	2.564(5)	S3–Ag1–S2^{ii}	110.7(2)
Ag1–S4	2.572(5)	S1^{i}–Ag1–S4	105.1(2)
		S3–Ag1–S4	109.4(2)
		S2^{ii}–Ag1–S4	108.7(2)
Ag2–S2	2.534(6)	S2–Ag2–S1^{iii}	111.1(1)
Ag2–S1^{iii}	2.556(5)	S2–Ag2–S4	109.9(2)
Ag2–S4	2.563(5)	S1^{iii}–Ag2–S4	108.0(2)
Ag2–S3^{i}	2.592(5)	S2–Ag2–S3^{i}	108.3(2)
		S1^{iii}–Ag2–S3^{i}	109.4(2)
		S4–Ag2–S3^{i}	110.3(1)
Sn–S1	2.399(4)	S1–Mn–S2	110.9(2)
Sn–S4	2.399(4)	S1–Mn–S3	106.6(3)
Sn–S2^{v}	2.401(4)	S2–Mn–S3	111.0(3)
Sn–S3^{ii}	2.405(4)	S1–Mn–S4^{iv}	110.2(3)
		S2–Mn–S4^{iv}	110.0(3)
		S3–Mn–S4^{iv}	108.1(2)
Mn–S1	2.404(7)	S1–Sn–S4	109.4(2)
Mn–S2	2.425(6)	S1–Sn–S2^{v}	110.9(1)
Mn–S3	2.427(6)	S4–Sn–S2^{v}	107.5(2)
Mn–S4^{iv}	2.454(8)	S1–Sn–S3^{ii}	108.5(2)
		S4–Sn–S3^{ii}	110.6(1)
		S2^{v}–Sn–S3^{ii}	109.9(2)

Symmetry codes used to generate equivalent atoms: (i) *x*–1, –*y*+1, *z*–1/2; (ii) *x*, –*y*+1, *z* + 1/2; (iii) *x*–1, –*y*, *z*–1/2; (iv) *x* + 1, *y*, *z*; (v) *x*, –*y*, *z* + 1/2.

crystal analysis, significantly better structural *R*-values were obtained for the monoclinic structure model. Figure 2 shows a plot of the refined diffraction pattern of Ag_2MnSnS_4. Further details on the measurement and refinement, as well as the refined atomic coordinates and isotropic displacement parameters can be found in the Tables S1 and S2 (Supporting Information).

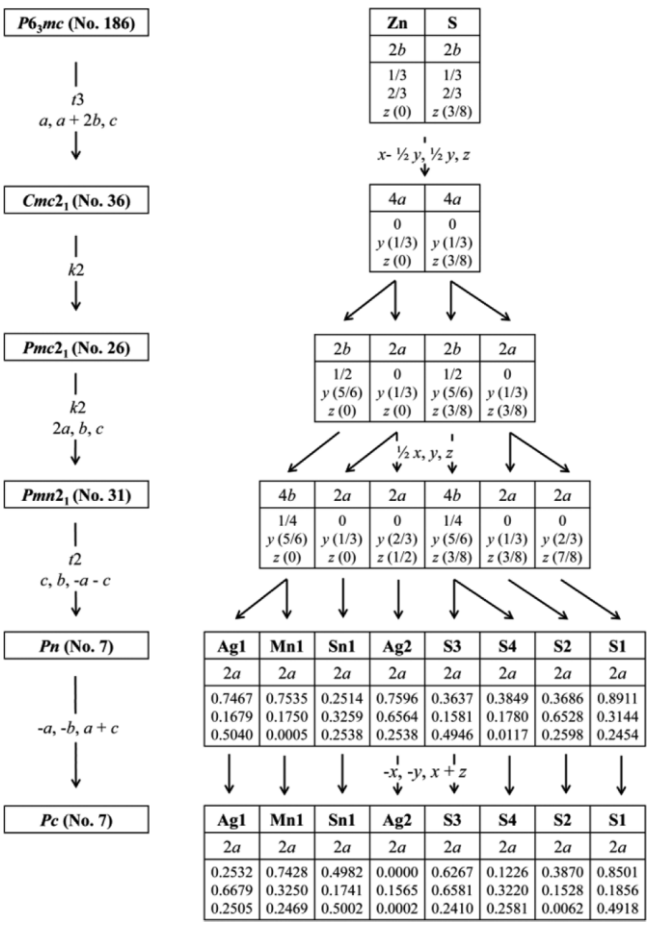

Figure 1. Bärnighausen-tree[40] showing the structure relations between the wurtzite structure and Ag_2MnSnS_4 in *Pn* and *Pc*, respectively.

© 0000 WILEY-VCH Verlag GmbH & Co. KGaA, Weinheim

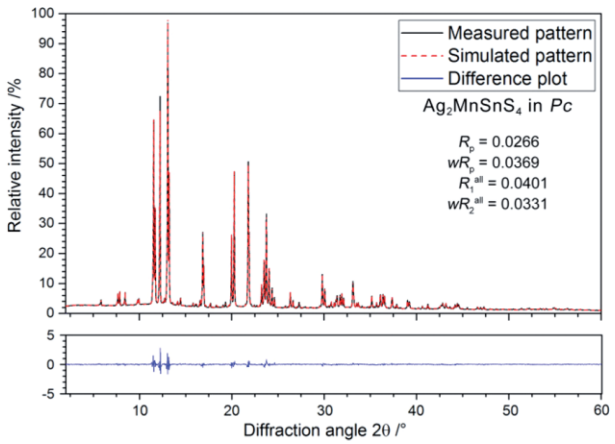

Figure 2. Rietveld refinement of the X-ray diffraction pattern of Ag_2MnSnS_4 (λ = 0.70930 Å, T = 20 °C, 0.3 mm glass capillary, 3885 data points) in the space group *Pc* including the difference plot.

An EDX analysis of the powdered, phase-pure substance used for the Rietveld refinement confirmed the sum formula of the compound Ag_2MnSnS_4 (see Figure S1, Table S3, Supporting Information).

Thermal Analysis

The possibility of a polymorphic phase transition of Ag_2MnSnS_4 from *Pn* to *Pmn*2_1 was studied using differential thermal analysis (DTA). The analysis revealed several thermal effects in the two heating- and cooling cycles (see Figure S2, Supporting Information). After the experiment, the sample color had changed from reddish brown to metallic gray. A phase analysis using X-ray diffraction after this analysis revealed a mixture of Ag_8SnS_6, MnS, and Ag_2MnSnS_4 as the minority phase, respectively. The high-temperature behavior was further confirmed by high- and low-temperature X-ray powder diffraction experiments (see Figure S3, Supporting Information). This analysis confirmed that Ag_2MnSnS_4 indeed decomposes at 700 °C and MnS remains as the sole detectable crystalline phase. Upon subsequent cooling below 520 °C, Ag_8SnS_6 also started to crystallize in the sample, confirming the results of the thermal analysis. Ag_2MnSnS_4 therefore has a peritectic decomposition temperature of approximately 700 °C.

Interestingly, a slight shift of several reflections of Ag_2MnSnS_4 can be observed when the compound is heated to temperatures above 400 °C. This could indicate a phase-transition to another polymorph with higher symmetry (e.g. orthorhombic symmetry), as observed for example in the parent compound Li_2MnSnS_4.[41] However, as the diffraction pattern only slightly changes compared to the ambient temperature modification, a Rietveld refinement of this phase could not confirm this higher symmetry. Thus, phase transitions to a sphalerite-type related phase as discussed in reference[34] can be ruled out based on our high-temperature diffraction studies.

Crystal Structure Description of Ag_2MnSnS_4

Ag_2MnSnS_4 is a normal valent adamantane structure according to the definition given by *Parthé*.[24] It crystallizes isopointal to other adamantane compounds like Li_2ZnSnS_4,[35] Li_2FeGeS_4,[42,43] Li_2FeSnS_4,[42,43] Ag_2FeSiS_4[42] or Li_2MnSnS_4,[41] with switched positions of the anions and cations. Ag_2MnSnS_4 contains two silver, one manganese, one tin, and four sulfur sites (Figure 3). Each sulfide anion (S1, S2, S3, S4) is located in a tetrahedral surrounding by Ag1, Ag2, Mn, and Sn. The Ag^+, Mn^{2+}, and Sn^{4+} cations are tetrahedrally coordinated by one of each of the independent sulfide anions (S1, S2, S3, S4).

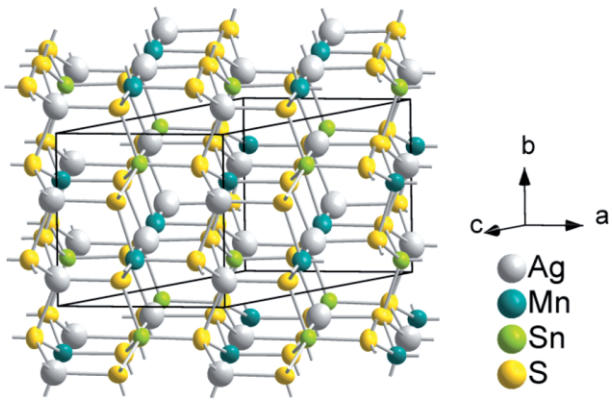

Figure 3. Section of the crystal structure of Ag_2MnSnS_4, showing the diamond-like arrangement of the atoms.

The crystal structure of Ag_2MnSnS_4 can be derived from the wurtzite type via cross-substitution by replacing the zinc cations with stoichiometric amounts of silver, manganese, and tin.[24]

The average volume differences were calculated according to the method of *Bernert* by comparison of the individual tetrahedra volumes with the average volume.[31] The values of the tetrahedra volumes are 8.54(5) Å^3 for Ag1, 8.62(5) Å^3 for Ag2, 7.33(5) Å^3 for Mn, and 7.10(4) Å^3 for Sn, which result in an average tetrahedral volume of 7.90 Å^3.[44] The individual values deviate from the average tetrahedral volume by 7.5 % for Ag1, 8.4 % for Ag2, 7.7 % for Mn, and 11.2 % for Sn. From these values, an average volume difference of 8.7 % is calculated for Ag_2MnSnS_4. This value lies in the region for hexagonal closest packed atoms. Therefore, the wurtzite type superstructure of Ag_2MnSnS_4 fits perfectly to the model presented by *Bernert*.[31] The volumes of the tetrahedra around S1, S2, S3, and S4 are almost identical with values of 7.70(5) Å^3 for S1, 7.83(5) Å^3 for S2, 7.93(5) Å^3 for S3, and 7.97(5) Å^3 for S4. This observation of similar volumes of the tetrahedra around the sulfide anions compared to the cation coordination polyhedra also holds true for the adamantane compounds mentioned above.[35,41–43]

Optical Properties

The optical bandgap of the dark red powdered substance was determined by UV/Vis diffuse reflectance spectroscopy (Figure 4). The absorption data was calculated using a modified Kubelka-Munk function.[45,46] Extrapolation of the linear part onto the baseline revealed an optical bandgap of 2.0 eV, which is in good agreement with the dark red color of the

 © 0000 WILEY-VCH Verlag GmbH & Co. KGaA, Weinheim

powdered substance and literature data. This value is slightly smaller than the optical bandgap of ca. 2.3 eV found in the analogous lithium compound Li_2MnSnS_4.[41]

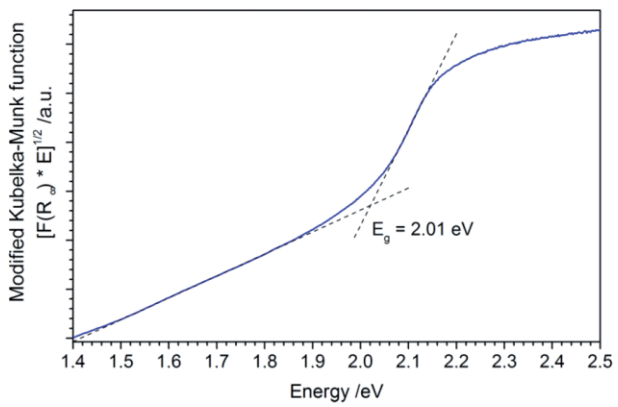

Figure 4. Diffuse reflectance spectrum of Ag_2MnSnS_4. The optical bandgap was determined by extrapolation of the linear part of the modified Kubelka-Munk function onto the baseline, which is indicated by the dashed lines.

Raman Spectroscopy

The Raman spectrum of Ag_2MnSnS_4 (see Figure 5) shows one very prominent vibration with a Raman shift of 337 cm^{-1}. This vibration can be attributed to the Sn–S stretching vibrations[47] in Ag_2MnSnS_4, while the less intense vibrations result from Mn–S and Ag–S stretching vibrations as well as deformation and lattice vibrations.

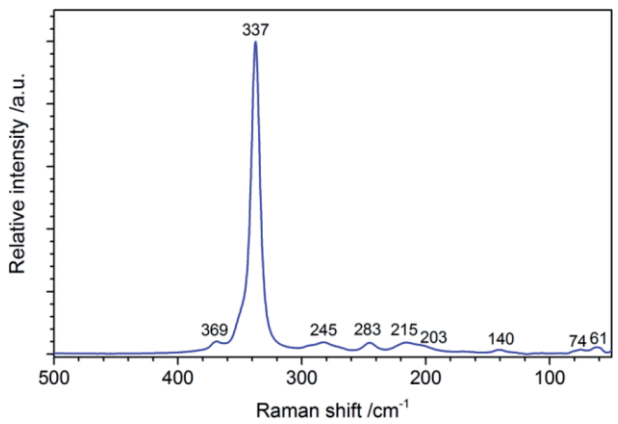

Figure 5. Raman spectrum of Ag_2MnSnS_4 (T = 25 °C, λ = 532 nm).

Magnetic Susceptibility Data

Figure 6 (top) shows the temperature dependence of the reciprocal magnetic susceptibility taken at a magnetic flux density of 10 kOe. The data was fitted according to a modified Curie–Weiss law in the temperature range from 50–310 K, leading to an experimental magnetic moment of μ_{exp} = 5.4(1) μ_B per manganese atom, a weak temperature independent contribution of χ_0 = –0.0016(1) emu·mol^{-1} (a diamagnetic impurity phase) and a Weiss constant of θ_P = –23.9(2) K. The experimental magnetic moment is slightly lower that the theoretical value of 5.92 μ_B for a Mn^{2+} cation in high-spin state. If one considers the intrinsic diamagnetic contribution of -290×10^{-6} emu·mol^{-1} for $(2Ag^+)Mn^{2+}Sn^{4+}(4S^{2-})$ (data taken from *Lueken*[48]), the similar fit results in a temperature independent contribution of χ_0 = –0.0013(1) emu·mol^{-1} without changing the value of the experimental magnetic moment, underlining the influence of the diamagnetic impurity phase and thus the reduced moment.

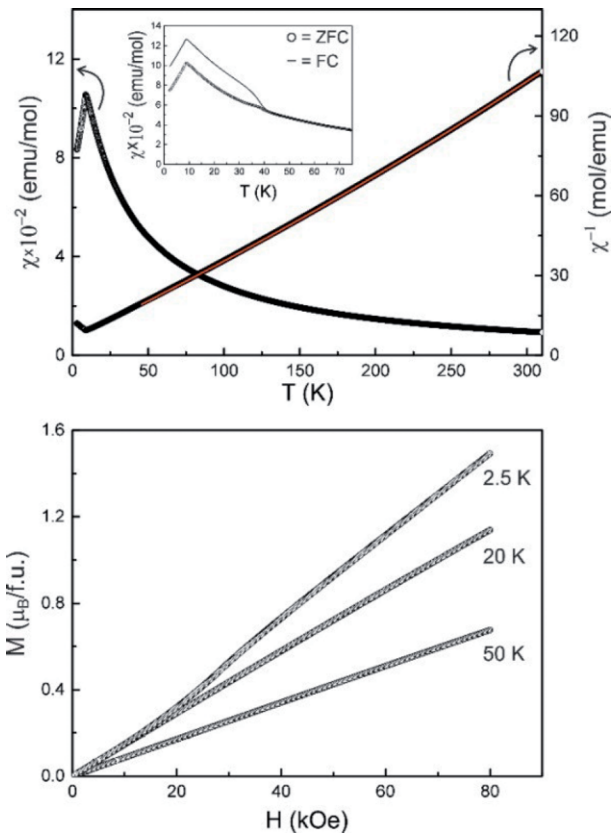

Figure 6. (top) Temperature dependence of the susceptibility measured with an applied field of 10 kOe in the temperature range of 3–300 K in ZFC mode. Fit of the inverse magnetic Susceptibility with a modified version of the Curie–Weiss law depicted in red; (inset) magnetic susceptibility measured in ZFC/FC mode with a magnetic flux density of 100 Oe; (bottom) magnetization isotherms measured in the magnetic field range of 0–80 kOe at 2.5, 20, and 50 K.

An additional measurement was performed in zero-field-cooled / field-cooled mode at 100 Oe (inset of Figure 6, top). The low-field data clearly manifest antiferromagnetic ordering of the manganese spins below a Néel temperature of T_N = 8.8(1) K. A second anomaly is detected at T_C = 40.2 K that can be ascribed to a yet unknown ferromagnetic impurity phase of very low quantity. The anomaly is already suppressed in the 10 kOe measurement. The magnetization behavior of Ag_2MnSnS_4 is shown in Figure 6 (bottom). At 20 and 50 K (well above the magnetic ordering temperature) we observe a linear increase of the magnetization as is usual for a paramagnetic material. The increase is at first also linear in the 2.5 K isotherm but at a critical field of H_C = 16(1) kOe we observe

© 0000 WILEY-VCH Verlag GmbH & Co. KGaA, Weinheim

a steeper increase. This metamagnetic step (antiparallel-to-parallel spin realignment) further manifests the antiferromagnetic ground state. The magnetization at 2.5 K and 80 kOe is μ_{sm} = 1.5(1) μ_B / f.u.

^{119}Sn Mössbauer Spectroscopy

The ^{119}Sn Mössbauer spectra of Ag_2MnSnS_4 at 6 and 78 K are presented in Figure 7 along with transmission integral fits. The 78 K spectrum shows a single signal at an isomer shift of δ = 1.34(1) mm·s^{-1} in close agreement with the crystal structure. The isomer shift nicely fits into the family of thiostannates(IV). A larger compilation of isomer shifts by *Lippens*[49] shows a quite narrow range from 1.1 to 1.4 mm·s^{-1}. The small deviation of the SnS_4 tetrahedra from ideal symmetry is reflected in a weak quadrupole splitting parameter of ΔE_Q = 0.27(3) mm·s^{-1}. The experimental line width of 0.93(2) mm·s^{-1} is in the usual range. Below the Néel temperature the signal becomes slightly broadened, resulting from a small transferred hyperfine field of B_{hf} = 1.02(1) T. Since the transferred field and the quadrupole splitting are small, independent refinement of these parameters was not possible (too large correlation). For fitting of the 6 K data the quadrupole splitting parameter was fixed at ΔE_Q = 0 mm·s^{-1}.

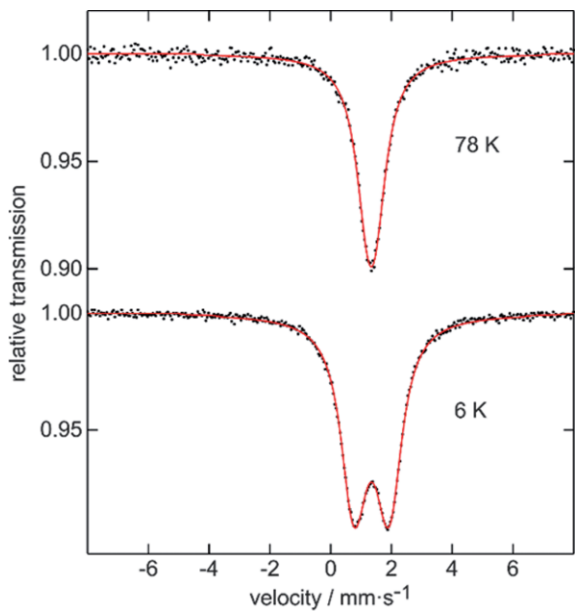

Figure 7. Experimental (black dots) and simulated (solid red lines) ^{119}Sn Mössbauer spectra of Ag_2MnSnS_4 at 6 and 78 K.

Conclusions

Ag_2MnSnS_4, a new diamond-like semiconductor was obtained from the elements by high-temperature synthesis in evacuated quartz glass ampoules. The compound is a red diamond-like semiconductor with an optical bandgap of ca. 2.0 eV. X-ray diffraction of phase-pure samples showed a (pseudo-)orthorhombic metric. The crystal structure of Ag_2MnSnS_4 is in fact monoclinic and the structure was solved from a pseudo-merohedrally twinned crystal. In order to confirm the monoclinic structure model, a Rietveld refinement of the X-ray diffraction pattern was performed. Both methods converged with significantly better *R* values for the monoclinic structure model as compared to the orthorhombic symmetry. The crystal structure of the title compound can be derived from the wurtzite structure type, which is in good accordance with the tetrahedral volume concept.[25–30] Ag_2MnSnS_4 is stable up to 700 °C and apparently undergoes a reversible phase-transition above 400 °C. Further details could not be resolved yet, but a transformation to a sphalerite-type modification can certainly be excluded.

Experimental Section

Synthesis of Ag_2MnSnS_4: Ag_2MnSnS_4 was prepared by heating stoichiometric amounts of silver (Ag, Chempur 99.9 %), manganese (Mn, Chempur 99.95 %), tin (Sn, Chempur 99+ %), and sulfur (S, Chempur 99.999 %) in evacuated quartz glass ampoules. After an initial heating process of 1 d at 400 °C, which is necessary to avoid a too high sulfur pressure, the ampoule was then heated to 800 °C for 1 d to ensure a complete reaction of the elements. Finally, the reaction mixtures were annealed at 500 °C for 8 d, homogenized by grinding, and subsequently annealed at 500 °C for several days.

Single-crystal X-ray Diffraction: Single-crystal X-ray diffraction data were collected with a STOE IPDS I using Mo-K_α radiation (λ = 0.71073 Å) radiation at ambient conditions. The diffraction data was corrected by a numerical absorption correction using X-SHAPE[37] and X-RED.[36] The resulting data had a completeness of 99.9 % within 25° θ. The crystal structure was solved by charge flipping methods using ShelXT[38] and refined on F^2 with ShelXL using full-matrix least-squares methods.[39] The experimental parameters and details of the structure solution and refinement are summarized in Table 1.

X-ray Powder Diffraction: The X-ray powder pattern used for the Rietveld refinement was collected with a STOE Stadi P diffractometer, equipped with a Dectris Mythen 1 K detector, using monochromatized Mo-$K_{\alpha1}$ radiation (λ = 0.70930 Å). The powdered sample was measured in Debye–Scherrer setup in a glass capillary (diameter 0.3 mm) in order to minimize preferred orientation effects on the reflection intensities. The Rietveld refinement was performed using Jana2006.[50] A manual background combined with 5 Legendre polynoms was used. The reflection profiles were described using a fundamental parameter approach and Pseudo Voigt functions, refining the parameters CSizeG and StrainL. The orthorhombic and monoclinic structure models obtained from the single-crystal measurements were used as starting models, however, the same models could also be obtained using charge flipping methods using SUPERFLIP.[51] The atomic coordinates and isotropic displacement parameters were refined without any restraints and converged straight forward.

In situ high-temperature measurements were performed using monochromatized Mo-$K_{\alpha1}$ radiation (λ = 0.70930 Å) and a STOE capillary furnace 0.65. The furnace temperature was controlled by a Eurotherm 24.16 controller (ΔT = ±1 °C). For the low-temperature measurements, an Oxford Cryosystems Cryostream 700 was used. The powdered sample was flame sealed in quartz glass capillaries (diameter 0.3 mm) for the temperature dependent measurements. Due to the furnace architecture, the capillary had to be placed in another 0.5 mm quartz glass capillary for the high-temperature measurements.

© 0000 WILEY-VCH Verlag GmbH & Co. KGaA, Weinheim

The diffraction data was collected in the range from 5.05° ≤ 2θ ≤ 23.92° with an irradiation time of 300 s in the temperature region from –150 °C to 25 °C and 25 °C to 850 °C in steps of 10 K (heating-/cooling rate 5 K·min^{-1}, 10 min annealing prior to each measurement). The STOE WinX^{POW} program package was used for the data collection and analysis.[52]

Further details of the crystal structure investigations may be obtained from the Fachinformationszentrum Karlsruhe, 76344 Eggenstein-Leopoldshafen, Germany (Fax: +49-7247-808-666; E-Mail: crysdata@fiz-karlsruhe.de, http://www.fiz-karlsruhe.de/request for deposited data.html) on quoting the depository number CSD-434389.

SEM/EDX Analysis: Quantitative EDX analysis was performed with a Zeiss EVO MA 15 SEM equipped with a Bruker Quantax EDX system with an X Flash Detector 630 M. A powdered sample of Ag_2MnSnS_4 (sputtered with an Au/Pd alloy) was analysed at three different positions with a voltage of 30 keV and an irradiation time of 120 s.

Thermal Analysis: The Differential thermal analysis (DTA) of Ag_2MnSnS_4 was performed with a SETARAM TG-DTA 92 16.18 in an evacuated quartz glass ampoule using Al_2O_3 as reference material. During the measurement two heating- and cooling-cycles were collected in the temperature range of 25–1000 °C with a heating- and cooling rate of 10 K·min^{-1}.

Raman Spectroscopy: The Raman spectrum was recorded with a Thermoscientific DXR™ SmartRaman spectrometer (excitation wavelength λ = 532 nm) in the range of 50–500 cm^{-1} with a resolution of 0.5 cm^{-1}.

UV/Vis Spectroscopy: Diffuse reflectance measurements were performed with a Bruins Omega 20 UV/Vis spectrometer using $BaSO_4$ as a white standard (100 % reflectance). The absorption spectrum was calculated using a modified Kubelka-Munk function.[45,46]

Magnetic Characterization: The investigation of the magnetic properties was carried out using a Quantum Design Physical Property Measurement System (PPMS) equipped with a Vibrating Sample Magnetometer (VSM). 39.413 mg of the sample were fixed in a polypropylene capsule and attached to a brass sample holder of the VSM. The measurements were performed in the temperature range of 2.5–310 K applying magnetic fields of up to 80 kOe.

Mössbauer Spectroscopy: A $Ca^{119m}SnO_3$ source was used for the Mössbauer spectroscopic experiments, which were carried out with a Continuous Flow Cryostat System (Janis Research Co LLC.) at 6 and 78 K. The Mössbauer source was kept at room temperature. The sample was enclosed in small PMMA containers at an optimized thickness. Fitting of the data was done by using the Normos-90 program package.[53]

Supporting Information (see footnote on the first page of this article): Table S1, S2 show details of the Rietveld refinement of Ag_2MnSnS_4, the atomic positions, and isotropic displacement parameters obtained from the Rietveld refinement. Figure S1 and Table S3 show the SEM/EDX analysis of Ag_2MnSnS_4. Figure S2 shows the thermal analysis (DTA) of Ag_2MnSnS_4. Figure S3 shows the low- and high-temperature X-ray diffraction patterns of Ag_2MnSnS_4 in the range of -150 to 850 °C.

Acknowledgements

The authors would like to thank *Prof. Dr. Manfred Scheer* (University of Regensburg) for the Raman spectroscopic measurements.

Keywords: Diamond-like semiconductor; Magnetic properties; Mößbauer spectroscopy; Non-ambient X-ray powder diffraction; Rietveld refinement

References

[1] L. O. Brockway, *Z. Kristallogr.* **1934**, *89*, 434–441.
[2] E. Parthé, K. Yvon, R. H. Deitch, *Acta Crystallogr., Sect. B* **1969**, *25*, 1164–1174.
[3] W. Schäfer, R. Nitsche, *Z. Kristallogr.* **1977**, *45*, 356–370.
[4] S. Harada, *Mater. Res. Bull.* **1973**, *8*, 1361–1369.
[5] N. A. Goryunova, J. C. Anderson (Eds.), *The Chemistry of Diamond-Like Semiconductors*, Chapman and Hall, London **1966**, *19*, 120.
[6] J. W. Lekse, M. A. Meghann, K. L. McNerny, J. Yeon, P. S. Halasyamani, J. A. Aitken, *Inorg. Chem.* **2009**, *48*, 7516–7518.
[7] S. Wagner, P. M. Bridenbaugh, *J. Cryst. Growth* **1977**, *39*, 151–159.
[8] S. Siebentritt, *Thin Solid Films* **2002**, *403*,1–8.
[9] L. Guen, W. S. Glaunsinger, A. Wold, *Naturwissenschaften* **1965**, *52*, 426–426.
[10] C. Steinhagen, M. G. Panthani, V. Akhavan, B. Goodfellow, B. Koo, B. A. Korgel, *J. Am. Chem. Soc.* **2009**, *131*, 12554–12555.
[11] J. J. Scragg, P. J. Dale, L. M. Peter, G. Zoppi, I. Forbes, *Phys. Status Solidi* **2008**, *245*, 1772–1778.
[12] L. K. Samanta, G. C. Bhar, *Phys. Status Solidi* **1977**, *41*, 331–337.
[13] D. A. Roberts, *Appl. Optics.* **1996**, *24*, 4677–4688.
[14] G. Catella, D. Burlage, *Mater. Res. Bull.* **1998**, *33*, 28–36.
[15] X. Li, C. Li, M. Zhou, Y. Wu, J. Yao, *Chem. Asian J.* **2017**, *24*, 3172–3177.
[16] J. A. Brant, D. J. Clark, Y. S. Kim, J. I. Jang, J.-H. Zhang, J. A. Aitken, *Chem. Mater.* **2014**, *26*, 3045–3048.
[17] D. Mei, W. Yin, K. Feng, Z. Lin, L. Bai, J. Yao, Y. Wu, *Inorg. Chem.* **2012**, *51*, 1035–1040.
[18] W. Yin, K. Feng, W. Hao, J. Yao, Y. Wu, *Inorg. Chem.* **2012**, *51*, 5839–5843.
[19] E. Honig, H. S. Shen, G. Q. Yao, K. Doverspike, R. Kershaw, K. Dwight, A. Wold, *Mater. Res. Bull.* **1988**, *23*, 307–312.
[20] L. Guen, W. S. Glaunsinger, A. Wold, *Mater. Res. Bull.* **1979**, *79*, 463–467.
[21] A. M. Lamarche, A. Willsher, L. Chen, G. Lamarche, J. C. Woolley, *J. Solid State Chem.* **1991**, *94*, 313–318.
[22] G. Nénert, T. T. M. Palstra, *J. Phys.: Condens. Matter* **2009**, *21*, 176002.
[23] a) A. Pfitzner, *Inorg. Chem.* **1998**, *37*, 5164–5167; b) A. Pfitzner, S. Reiser, T. Nilges, W. Kockelmann, *J. Solid State Chem.* **1999**, *147*, 170–176.
[24] E. Parthé in *Crystal Structures of Intermetallic Compounds* (Eds.: J. H. Westbrook, R. L. Fleischer), J. Wiley and Sons, New York, **2000**, vol. 1, 117–137.
[25] A. Pfitzner, S. Reiser, *Z. Kristallogr.* **2002**, *217*, 51–54.
[26] T. Bernert, A. Pfitzner, *Z. Anorg. Allg. Chem.* **2002**, *628*, 2161.
[27] M. Robbins, M. A. Miksovsky, *J. Solid State Chem.* **1972**, *5*, 462–466.
[28] M. E. Fleet, *Mater. Res. Bull.* **1976**, *11*, 11179–11183.
[29] A. Pfitzner, T. Bernert, *Z. Kristallogr.* **2004**, *219*, 20–26.
[30] T. Bernert, A. Pfitzner, *Z. Anorg. Allg. Chem.* **2004**, *630*, 1711.
[31] T. Bernert, A. Pfitzner, *Z. Kristallogr.* **2005**, *220*, 968–972.
[32] T. Bernert, A. Pfitzner, *Z. Anorg. Allg. Chem.* **2006**, *632*, 1213–1218.
[33] J. W. Lekse, PhD Thesis, Duquesne University **2009**.
[34] G. E. Delgado, N. Sierralta, M. Quintero, E. Quintero, E. Moreno, J. A. Flores-Cruz, C. Rincón, *Rev. Mex. Fís.* **2018**, *64*, 216–221.
[35] J. W. Lekse, B. M. Leverett, C. H. Lake, J. A. Aitken, *J. Solid State Chem.* **2008**, *181*, 3217–3222.
[36] X-RED32, STOE & Cie GmbH, **2004**.

 © 0000 WILEY-VCH Verlag GmbH & Co. KGaA, Weinheim

[37] X-Shape, STOE & Cie GmbH, **1999**.
[38] G. M. Sheldrick, *Acta Crystallogr., Sect. A* **2015**, *71*, 3–8.
[39] G. M. Sheldrick, *Acta Crystallogr., Sect. C* **2015**, *71*, 1–2.
[40] H. Bärnighausen, *MATCH Commun. Math. Chem.* **1980**, *9*, 139–175.
[41] K. P. Devlin, A. J. Glaid, J. A. Brant, J.-H. Zhang, M. N. Smec, D. J. Clark, Y. S. Kim, J. I. Jang, K. R. Daley, M. A. Moreau, J. D. Madura, J. A. Aitken, *J. Solid State Chem.* **2015**, *231*, 256–266.
[42] C. D. Brunetta, J. A. Brant, K. A. Rosmus, K. M. Henline, E. K. J. H. MacNeil, J. A. Aitken, *J. Alloys Compd.* **2013**, *574*, 495–503.
[43] S. Azam, S. A. Khan, S. Goumri-Said, *Solid State Sci.* **2017**, *72*, 71–79.
[44] T. Balic Zunic, I. Vickovic, *J. Appl. Crystallogr.* **1996**, *29*, 305–306.
[45] P. Kubelka, F. Munk, *Z. Techn. Physik* **1931**, 593.
[46] H. Kisch, *Angew. Chem. Int. Ed.* **2013**, *52*, 812–847.
[47] A. J. Smith, P. E. Meek, W. Y. Liang, *J. Phys. C: Solid State Phys.* **1977**, *10*, 1321–1333.
[48] H. Lueken, *Magnetochemie*, Teubner, Stuttgart, **1999**.
[49] P. E. Lippens, *Phys. Rev. B* **1999**, *60*, 4576–4586.
[50] V. Petricek, M. Dusek, L. Palatinus, *Z. Kristallogr.* **2014**, *229*, 345–352.
[51] L. Palatinus, G. Chapuis, *J. Appl. Crystallogr.* **2007**, *40*, 789–790.
[52] STOE WinX^{POW}, Version 3.10, STOE & Cie GmbH, Darmstadt 2016.
[53] R. A. Brand, Normos Mössbauer Fitting Program, University of Duisburg, Duisburg, Germany **2002**.
[54] F. Keutsch, D. Topa, R. Fredrickson, E. Makovicky, W. Paar, Mineralogical Magazine **2018**, 1-19, DOI: 10.1180/mgm.2018.139, Accepted Article.

Received: April 12, 2018
Published online: ■

 © 0000 WILEY-VCH Verlag GmbH & Co. KGaA, Weinheim

Journal of Inorganic and General Chemistry
ZAAC
Zeitschrift für anorganische und allgemeine Chemie

*D. Friedrich, S. Greil, T. Block, L. Heletta, R. Pöttgen, A. Pfitzner** **1–9**

Synthesis and Characterization of Ag_2MnSnS_4, a New Diamond-like Semiconductor

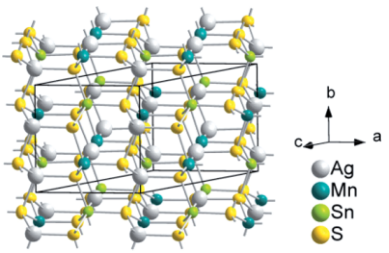

 © 0000 WILEY-VCH Verlag GmbH & Co. KGaA, Weinheim